Quantum and quasi-classical effects in the strong field ionization and subsequent excitation of nitrogen molecules

Liang Xu, Qi Lu, Vladimir T Tikhonchuk, Bin Zhou, Runzhe Yang, Qingqing Liang, Feng He, Rostyslav Danylo, Aurélien Houard, André Mysyrowicz, et al.

Research Article | Vol. 30, No. 21 / 10 Oct 2022 / Optics Express 38481
Optics EXPRESS

Quantum and quasi-classical effects in the strong field ionization and subsequent excitation of nitrogen molecules

LIANG XU,[1,*] QI LU,[1] VLADIMIR T. TIKHONCHUK,[2,3] BIN ZHOU,[1] RUNZHE YANG,[1] QINGQING LIANG,[1] FENG HE,[4,5] ROSTYSLAV DANYLO,[6] AURÉLIEN HOUARD,[6] ANDRÉ MYSYROWICZ,[6] AND YI LIU[1,5,7]

[1]*Shanghai Key Lab of Modern Optical System, University of Shanghai for Science and Technology, 200093 Shanghai, China*
[2]*University of Bordeaux-CNRS-CEA, CELIA, UMR 5107, 33405 Talence, France*
[3]*ELI-Beamlines Center, Institute of Physics, Czech Academy of Sciences, 25241 Dolní Břežany, Czech Republic*
[4]*Key Laboratory for Laser Plasmas (Ministry of Education) and School of Physics and Astronomy, Collaborative innovation center of IFSA (CICIFSA), Shanghai Jiao Tong University, Shanghai 200240, China*
[5]*CAS Center for Excellence in Ultra-intense Laser Science, Shanghai 201800, China*
[6]*Laboratoire d'Optique Appliquée, ENSTA Paris, Ecole Polytechnique, CNRS, Institut Polytechnique de Paris, 91762 Palaiseau cedex, France*
[7]*yi.liu@usst.edu.cn*
[*]*liangxu2021@usst.edu.cn*

Abstract: The processes leading to the N_2^+ lasing are rather complex and even the population distribution after the pump laser excitation is unknown. In this paper, we study the population distribution at electronic and vibrational levels in N_2^+ driven by ultra-short laser pulse at the wavelengths of 800 nm and 400 nm by using the quantum-mechanical time-domain incoherent superposition model based on the time-dependent Schrödinger equation and the quasi-classical model assuming instantaneous ionization injection described by density matrix. It is shown that while both models provide qualitatively similar results, the quasi-classical instantaneous ionization injection model underestimates the population inversions corresponding to the optical transitions at 391 nm, 423 nm and 428 nm due to the assumption of quantum mixed states at the ionization time. A fast and accurate correction to this error is proposed. This work solidifies the theoretical models for population at vibrational states in N_2^+ and paves the way to uncover the mechanism of the N_2^+ lasing.

1. Introduction

Optical amplification and lasing in air plasma pumped by intense laser pulses was reported for the first time in Refs. [1,2] and has attracted much attention due to its potential application in standoff spectroscopy [3] and remote sensing [4,5]. The three major atmospheric species, nitrogen, oxygen and argon, have been proven to produce such a lasing action. For all the three gases, both backward and forward lasing emissions have been observed and the relevant mechanisms have been discussed. Lasing emissions from neutral nitrogen molecules and atomic oxygen and argon have been largely understood [1,6,7]. By contrast, the physical mechanism of N_2^+ lasing is rather complex and controversial. Many investigations have been devoted to the existence of population inversion, the temporal shape of emission, the dependence on laser polarization, the contributions of molecular rotational and vibrational states, etc. The fundamental problem consists in evaluation of the population at different electronic and vibrational levels after the end

#469492 https://doi.org/10.1364/OE.469492
Journal © 2022 Received 5 Jul 2022; revised 14 Sep 2022; accepted 17 Sep 2022; published 3 Oct 2022

Optics EXPRESS

of the laser pulse, where strong field ionization and excitation processes occur simultaneously and compete with each other. A variety of different explanations have been proposed [8–16] but no consensus is obtained yet on their relative importance. Two main methods have been employed to address this problem: either by solving the time-dependent Schrödinger equation (TDSE) or by solving the density matrix (DM) equations.

TDSE is widely used in ultra-fast science and attosecond physics including strong field ionization, photo-dissociation, high harmonic generation, and air lasing. Yao et al. [8] attributed a fast population inversion between $B^2\Sigma_u^+$ and $X^2\Sigma_g^+$ to a significant transfer of population from the ground $X^2\Sigma_g^+$ state to $A^2\Pi_u$ state, but the initial ionization has been assumed artificially. Based on the time-domain incoherent superposition model, Xu et al. [9] suggested that the population inversion is achieved by post-ionization couplings among the lowest three electronic states of N_2^+. Ando et al. [17] by solving TDSE demonstrated that the coherent rovibrational population transfer between $X^2\Sigma_g^+$, $A^2\Pi_u$, and $B^2\Sigma_u^+$ electronic states of N_2^+ contributes to the population inversion. Moreover, by considering only an instantaneous ionization at the maximum of the laser pulse, some authors showed that the polarization-modulated intense laser pulse results in giant enhancement of air lasing due to excessive population inversion [18,19].

The density matrix equations are widely used in quantum optics. In contrast to TDSE, DM has advantages on dealing with quantum mixed states and being more efficient numerically. Zhang et al. [20] introduced an instantaneous ionization injection model by considering several vibrational levels and investigated the interwoven dynamics of N_2^+ ion in an intense laser field. Tikhonchuk et al. [21] extended the model to include subsequent lasing amplification process in the plasma by considering the Maxwell-Bloch equations. It was concluded that populations of the N_2^+ excited levels depend significantly on such laser parameters as intensity and wavelength [22].

Since the population distribution at different electronic and vibrational levels of N_2^+ after excitation by the strong laser field is fundamental for uncovering the underlying mechanism of N_2^+ lasing, it is instructive to understand how accurate is the reduced DM model compared to the coherent quantum-mechanical description. In this paper, we perform a quantitative comparison between the time-domain incoherent superposition model based on TDSE [9] and the instantaneous ionization injection model with a limited number of excited levels described by density matrix [20–22]. Both models include ionization and excitation of nitrogen molecules induced by the whole laser field. We first simulate the vibrational population distribution of N_2^+ under an 800 nm laser pulse by using the two models and identify the similarities and differences. We find that the instantaneous ionization injection model described by density matrix underestimates the population inversion due to the transient ionization injection of mixed states. This error can be corrected by including off-diagonal elements in the ionization matrix accounting for the ionization in pure quantum states, thus providing a good agreement between these two complementary approaches, TDSE and DM. Then the influence of laser intensity on the population inversions responsible for the 391 nm and 428 nm emissions is discussed in detail and the role of ionization depletion for the higher intensity regime is identified. We also consider the population distribution of N_2^+ pumped by a 400 nm laser pulse and reveal that the single-photon pumping and instantaneous ionization injection together lead to the population inversions associated with 428 nm and 423 nm lasing. This paper is organized as follows. In Sec. 2, we introduce two numerical models, and the simulation results and discussions are given in Sec. 3. Conclusions are presented in Sec. 4.

Optics EXPRESS

2. Models of molecular ionization and excitation by an intense laser pulse

2.1. Time-domain incoherent superposition model based on the time-dependent Schrödinger equation

Under the Born-Oppenheimer approximation, a N_2^+ wave packet is expressed as:

$$\psi(\mathbf{r}, R; t) = \chi_X(R; t)\varphi_X(\mathbf{r}, R) + \chi_A(R; t)\varphi_A(\mathbf{r}, R) + \chi_B(R; t)\varphi_B(\mathbf{r}, R), \tag{1}$$

where $\mathbf{r}$ and R are the electron displacement and the internuclear distance, respectively; functions $\varphi_M(\mathbf{r}, R)$ denote the lowest three N_2^+ electronic states $M = X$, A or B, the higher electronic states are neglected due to large energy gaps. $\chi_M(R; t)$ are the corresponding nuclear vibrational wave packets, which are governed by the three-component time-dependent Schrödinger equation (Hartree atomic units are used throughout unless stated otherwise):

$$\frac{\partial}{\partial t}\begin{pmatrix} \chi_X(R,t) \\ \chi_A(R,t) \\ \chi_B(R,t) \end{pmatrix} = -i\,(H_0 + H_I)\begin{pmatrix} \chi_X(R,t) \\ \chi_A(R,t) \\ \chi_B(R,t) \end{pmatrix}, \tag{2}$$

with the field-free Hamiltonian H_0 is defined as

$$H_0 = \begin{pmatrix} P_R^2/2M_n + V_X(R) & 0 & 0 \\ 0 & P_R^2/2M_n + V_A(R) & 0 \\ 0 & 0 & P_R^2/2M_n + V_B(R) \end{pmatrix}. \tag{3}$$

Here, $M_n = 12852$ a.u. is the reduced nuclear mass of N_2^+, and P_R is the nuclear momentum operator, $V_M(R)$ represents the ion potential energy for the corresponding electronic state [23,24], as shown in Fig. 1(a).

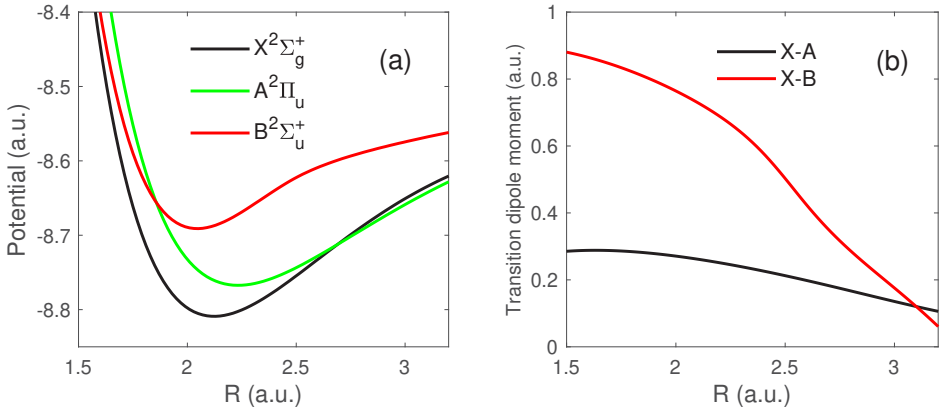

Fig. 1. (a) N_2^+ potential energy curves for the three electronic states $X^2\Sigma_g^+$ (black), $A^2\Pi_u$ (green), and $B^2\Sigma_u^+$ (red). (b) N_2^+ electronic transition dipole moments μ_{XA}^e for $X^2\Sigma_g^+$-$A^2\Pi_u$ (black) and μ_{XB}^e for $X^2\Sigma_g^+$-$B^2\Sigma_u^+$ (red). The data are taken from Refs. [23,24].

Optics EXPRESS

The interaction Hamiltonian H_I in the electric dipole approximation is written as

$$H_I = \begin{pmatrix} 0 & H_{XA} & H_{XB} \\ H_{XA} & 0 & 0 \\ H_{XB} & 0 & 0 \end{pmatrix}, \tag{4}$$

where $H_{XA} = -\mu^e_{XA}(R)E(t)\sin\theta$ and $H_{XB} = -\mu^e_{XB}(R)E(t)\cos\theta$ correspond to the perpendicular and parallel transitions, respectively, and θ is the angle between the laser electric field and molecular axis. The radial dependences of electronic transition dipole moments $\mu^e_{XA}(R)$ and $\mu^e_{XB}(R)$ are shown in Fig. 1(b) [23,24]. A linearly polarized laser field $E(t)$ is expressed as

$$E(t) = E_0\ \cos(\omega t)\ \sin^2(\pi t/\tau), \tag{5}$$

where E_0, ω, and τ refer to the amplitude, angular frequency, and duration of the laser pulse with a $\sin^2$ envelope, respectively.

Equation (2) is solved by using the Crank-Nicholson technique [25] with the time step $dt = 0.05$ a.u.. The one-dimensional spatial range of simulation is $[0, 4.4]$ a.u. with 220 data points. This simulation box is big enough to contain all wave packets and thus no absorbing boundaries are needed. The nuclear wave packet $\chi_M(\theta, R)$ for a given angle θ is initialized at the time moment of ionization t_i as a superposition of the vibrational eigenstates $\phi^\nu_M(R)$:

$$\chi_M(\theta, R; t_i) = \sum_\nu C^\nu_M(\theta, t_i)\phi^\nu_M(R). \tag{6}$$

The weight coefficients are calculated according to the ionization rate

$$C^\nu_M(\theta, t_i) = \left\{q^\nu_M w^\nu_M(\theta, E(t_i))\,[1 - n_{N_2^+}(t_i)]\right\}^{1/2}, \tag{7}$$

where q^ν_M is the Franck-Condon factor corresponding to ionization from the N_2 ground state into the $N_2{}^+$ electronic state M at the vibrational level ν. The ionization rate $w^\nu_M(\theta, E)$ depends on the corresponding ionization energy $I_p^{M\nu}$, and it is calculated according to the molecular Ammosov-Delone-Krainov theory [26,27]. The factor $1 - n_{N_2^+}(t_i)$ accounts for the remaining probability of the neutral molecule N_2, and $n_{N_2^+}$ represents the total ionization probability of N_2 before t_i. The vibrational eigenfunctions, $\phi^\nu_M(R)$, the Franck-Condon factors, q^ν_M, and the ionization energies, $I_p^{M\nu}$, have been obtained by using the imaginary time propagation method [28] and also been checked by the matrix diagonalization method. The Franck-Condon factors and ionization energies for the considered levels are listed in Table S1 in Supplement 1.

The simulations were performed from t_i to the end of the laser pulse t_{end} and the final population distribution is obtained via the incoherent addition over ionization time t_i and averaging over the alignment angle θ:

$$\bar{P}^\nu_M = \frac{1}{2}\int_0^\pi \sin\theta\, d\theta \int_0^{t_{\text{end}}} \left|\langle\phi^\nu_M(R)\mid \chi_M(\theta, R; t_i, t_{\text{end}})\rangle\right|^2\, dt_i. \tag{8}$$

This time-domain incoherent superposition model based on the time-dependent Schrödinger equation is abbreviated **TDSE model** in the rest of this paper. Convergence of the calculations has been tested by using finer spatial and time steps, whereas almost identical results were obtained.

Optics EXPRESS

2.2. Instantaneous ionization injection model with limited levels described by density matrix

The dynamics of the ionization of N_2 and excitation of N_2^+ can be also described by the time-dependent density matrix ρ, which is governed via the Bloch equations [20,21,29]

$$\frac{d\rho}{dt} = -i[H, \rho] + W. \tag{9}$$

Here, the diagonal elements $H^{\nu\nu}_{MM} = \mathcal{E}^{\nu}_{M}$ of the Hamiltonian H correspond to the energies of vibrational eigenstates. The off-diagonal elements are defined as $H^{\nu\nu'}_{XA} = -\mu^{\nu\nu'}_{XA} E(t) \sin\theta$ for the perpendicular interaction between $X^2\Sigma_g^+$ and $A^2\Pi_u$ states, and as $H^{\nu\nu'}_{XB} = -\mu^{\nu\nu'}_{XB} E(t) \cos\theta$ for the parallel interaction between $X^2\Sigma_g^+$ and $B^2\Sigma_u^+$ states. Eigenenergies $\mathcal{E}^{\nu}_{M}$ and transition dipole moments $\mu^{\nu\nu'}_{MM'}$ are calculated by the matrix diagonalization method and the latter is obtained by integrating over the radial wave functions of the corresponding states:

$$\mu^{\nu\nu'}_{XM} = \langle \phi^{\nu}_{X}(R) | \mu^{e}_{XM}(R) | \phi^{\nu'}_{M}(R) \rangle \tag{10}$$

with $M = A$ for the perpendicular interaction and $M = B$ for the parallel interaction. The results were double checked by the technique of the imaginary time propagation in TDSE. The values are reported in Tables S2 and S3 in Supplement 1.

The second term W on the right-hand side in Eq. (9) accounts for the field-induced ionization from N_2 to N_2^+. It has only diagonal elements $W^{\nu\nu}_{MM}$ calculated according to the molecular Ammosov-Delone-Krainov theory [26,27]

$$W^{\nu\nu}_{MM}(t) = |C^{\nu}_{M}(t)|^2. \tag{11}$$

In total, 19 vibrational levels are considered: 5 levels for the $X^2\Sigma_g^+$ state with $\nu = 0-4$, 7 levels for the $A^2\Pi_u$ state with $\nu = 0-6$ and 7 levels for the $B^2\Sigma_u^+$ state with $\nu = 0-6$. Equation (9) is solved by using the fixed-step fourth-order Runge-Kutta technique with the time step $dt = 0.05$ a.u. with the laser field given by Eq. (5) and with zero initial condition $\rho(\theta, t = 0) = 0$. The simulations have been performed with angles θ ranging from 0 to π and the diagonal elements are averaged over the molecular orientation

$$\bar{P}^{\nu}_{M} = \frac{1}{2} \int_0^{\pi} \rho^{\nu\nu}_{MM}(\theta, t_{\text{end}}) \sin\theta \, d\theta. \tag{12}$$

These diagonal elements represent the population at ν vibrational states. The instantaneous ionization injection model described by density matrix is denoted as **DM model**. The numerical convergence of this model have been checked by using more excited levels and finer time steps.

3. Results and discussions

3.1. Comparison of the TDSE and DM models

Lasing at 391 and 428 nm in molecular nitrogen irradiated by an intense 800 nm laser pulse was reported in Refs. [2,8,9,11]. These coherent emissions correspond to transitions from the excited state $B^2\Sigma_u^+(\nu = 0)$ to the ground states $X^2\Sigma_g^+(\nu = 0, 1)$ of the N_2^+ molecule, respectively. Ionization of the neutral nitrogen and subsequent excitation of the nitrogen ion are the key processes that define the possibility of lasing after the end of laser pulse. Ionization itself cannot provide the population inversion needed for lasing. The results from both models are shown in Fig. 2(a) for the laser pulse duration equal 15 optical cycles, $\tau = 15\, T_{800}$. Due to large energy separation of excited levels from the N_2^+ ground state compared to the photon energy, ionization at the level $X^2\Sigma_g^+(\nu = 0)$ dominates. About 80% ions are in the ground state and population at

Optics EXPRESS

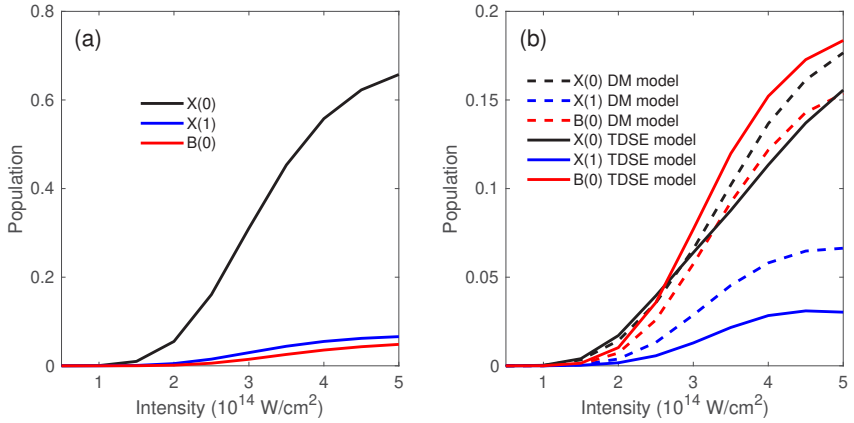

Fig. 2. N_2^+ population distribution at $X^2\Sigma_g^+$ vibrational states ($\nu = 0$ black and $\nu = 1$ blue) and $B^2\Sigma_u^+$ vibrational state ($\nu = 0$ red) as a function of the laser peak intensity. (a) considering only the N_2 ionization. In this case, TDSE and DM models provide the same results. (b) taking into account of both ionization and excitation processes. The solid and dashed lines represent the results predicted by TDSE and DM models, respectively. The laser parameters for (a) and (b): $\omega = 0.057$ a.u. ($\lambda = 800$ nm) and $\tau = 15\,T_{800}$ (where $T_{800} = 110.26$ a.u. is the laser period).

$X^2\Sigma_g^+(\nu = 1)$ level is larger than that at $B^2\Sigma_u^+(\nu = 0)$ level. Both TDSE and DM models provide the same results.

The situation changes dramatically when ionization and excitation are included simultaneously. The results calculated with two models are distinctly different, as demonstrated in Fig. 2(b). Solid and dashed lines denote TDSE and DM results, respectively. Although both models show qualitatively similar trends, there are significant quantitative differences. With increase of the laser intensity, the population at $B^2\Sigma_u^+(\nu = 0)$ level (red lines) increases for both two models. However, the TDSE model predicts an inversion between $B^2\Sigma_u^+(\nu = 0)$ and $X^2\Sigma_g^+(\nu = 0)$ levels for the laser intensity above 2.6×10^{14} W/cm^2, which is responsible for 391 nm lasing. This inversion can be attributed to the role of $A^2\Pi_u$ state, which serves as a "population reservoir" [8,9]. In contrast, no inversion for 391 nm transition is predicted by DM model. Both models predict inversion between $B^2\Sigma_u^+(\nu = 0)$ and $X^2\Sigma_g^+(\nu = 1)$ levels, which is responsible for the emission at 428 nm. However, TDSE model predicts a larger inversion. Moreover, we also observe that TDSE model shows a tend for saturation of the population at $B^2\Sigma_u^+(\nu = 0)$ level as the laser intensity increases, which is different from the results presented in Ref. [9]. This issue is discussed below in Sec. 3.2.

To better understand the difference between TDSE and DM models, we consider a representative case of $\theta = 45°$ and trace the population evolution with time in Fig. 3(a) for the laser intensity $I = 3.5 \times 10^{14}$ W/cm^2 and other parameters same as in Fig. 2. We can see that a large fraction of the population at $X^2\Sigma_g^+(\nu = 0)$ level is promoted to $A^2\Pi_u(\nu = 2)$ level (green line) through the single photon resonance and the population at $B^2\Sigma_u^+(\nu = 0)$ level increases due to the direct three-photon coupling. However, the population at $B^2\Sigma_u^+(\nu = 0)$ level, according to the TDSE model (red solid lines), is always larger than the DM model prediction (red dashed lines). After the end of laser pulse, the predicted popualtion inversions are 16% and 8% for both models. Note that populations at $X^2\Sigma_g^+$ levels attain maximum around the peak of laser pulse and decrease afterwards. By contrast, populations at $A^2\Pi_u$ and $B^2\Sigma_u^+$ levels increase monotonously with time.

It is known that the DM equations stem from TDSE and both models are equivalent for pure quantum states. But the DM method has an advantage to describe mixed states. In the TDSE

Optics EXPRESS

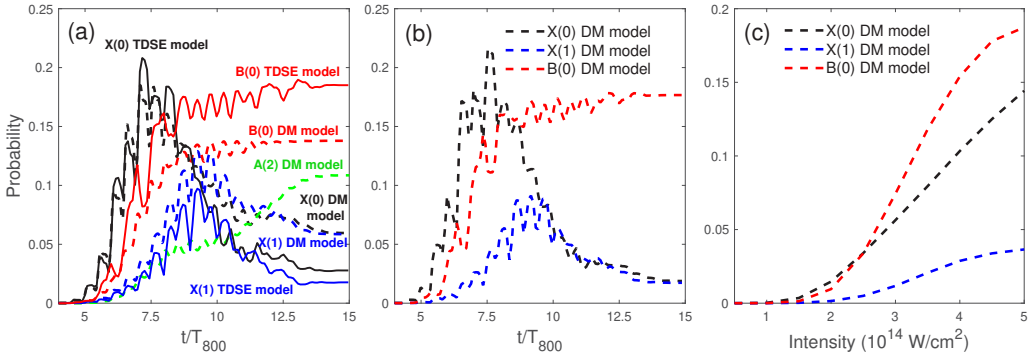

Fig. 3. (a) and (b) N_2^+ time-dependent excitation probabilities for the simulation with $\theta = 45°$ at the levels $X^2\Sigma_g^+$ ($v = 0$ black, $v = 1$ blue) and $B^2\Sigma_u^+$ ($v = 0$ red). (a) solid and dashed lines present the results of TDSE and DM models, respectively. (b) the results of DM model with the initial conditions including diagonal (9) and non-zero off-diagonal elements (13). Laser intensity is 3.5×10^{14} W/cm^2, other parameters in panels (a) and (b) are same as in Fig. 2. (c) Angle-averaged N_2^+ population distribution as a function of the laser peak intensity. The initial condition and other parameters are same as in panel (b).

model, according to the initial condition Eq. (7), at the ionization moment, the N_2^+ ion is prepared in a pure coherent state by the strong laser field. The TDSE model is run for different ionization times t_i and different angles θ, and at the end of laser pulse, the population probabilities are added incoherently according to Eq. (8). The situation is different for the DM model. According to Eq. (9), the transient ionization injection rate contains only diagonal elements W_{MM}^{vv}. That implies that many incoherent vibrational wave packets are created at the ionization time. These mixed ion states due to uncontrolled ionization are at the origin of the differences between the two models.

To confirm our hypothesis, we performed the DM simulations for Eq. (9) not only with the same initial diagonal elements but also with non-zero initial off-diagonal elements of the density matrix:

$$W_{MM'}^{vv'}(\theta, t) = C_M^{v*}(\theta, t)\, C_{M'}^{v'}(\theta, t), \tag{13}$$

where M and M' are equal to X, A or B and $v \neq v'$ if $M = M'$. The weight coefficients $C_M^v(\theta, t)$ are defined by Eq. (7). The time-dependent probability distribution is shown in Fig. 3(b). The value of population at $B^2\Sigma_u^+(v = 0)$ level (red dashed line) at the end of pulse is about 0.18 and very close to that calculated by the TDSE model: red solid line in Fig. 3(a). The populations at levels $X^2\Sigma_g^+(v = 0)$ and $X^2\Sigma_g^+(v = 1)$ corresponding to emissions at 319 nm and 428 nm are also very close to the TDSE results in Fig. 3(a).

The results of calculation of the population for all molecular orientations with the DM model using the initial condition Eqs. (9) and (13) is shown in Fig. 3(c). It is also in good agreement with the TDSE results shown in Fig. 2(b). The small deviations can be explained by the contribution of higher levels, which are inherently included in the TDSE model. Thus, we conclude that the original DM model in Sec. 2.2 underestimates the populations at excited levels due to the incoherent ionization injection. This deficiency of the original DM model can be corrected by adding off-diagonal elements in the ionization matrix according to Eq. (13). Such an improved DM model is in good agreement with the TDSE model while showing a good computational performance. Indeed, if there are N discrete time points in simulations, TDSE model need to be executed N times to get the complete population distribution at the end of the laser pulse. By contrast, one obtains almost the same results by performing one simulation with the corrected DM model.

Optics EXPRESS

3.2. Dependence of population inversion on the laser intensity and wavelength

According to the common understanding, the population transfer from $X^2\Sigma_g^+(v=0)$ to $A^2\Pi_u(v=2)$ level by the 800 nm laser pulse is due to the single photon excitation. It is proportional to the laser intensity. A larger population inversion and a stronger lasing are more likely to be achieved by using a higher intensity laser pulse. However, we found that this is not always true. Dependence of the population inversions corresponding to the transitions at 391 nm and 428 nm is shown in Fig. 4. Population inversion for the transition at 428 nm (red line) occurs at very low laser intensity of 1.5×10^{14} W/cm^2, and it increases monotonously with the laser intensity. By contrast, population inversion corresponding to the transition at 391 nm (blue line) is negative at low intensities and becomes positive for $I>2.6\times10^{14}$ W/cm^2. This non-monotonous behavior can be explained as a competition between the ionization injection and the excitation of vibrational levels.

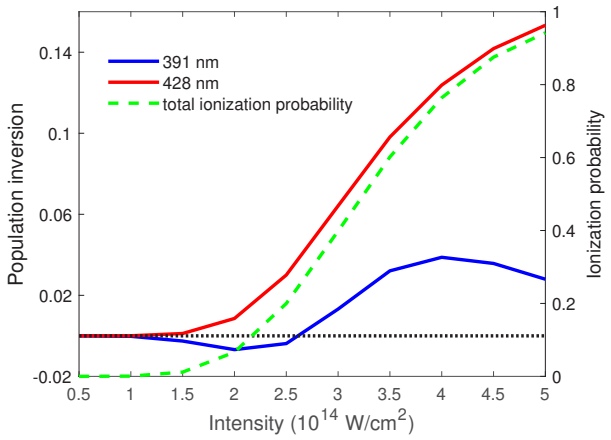

Fig. 4. Dependence of the population inversion (left axis) and the ionization probability (right axis) on the laser intensity calculated by the TDSE model. Blue line shows the population inversion between $B^2\Sigma_u^+(v=0)$ and $X^2\Sigma_g^+(v=0)$ levels corresponding to the transition at 391 nm. Red line shows the inversion between $B^2\Sigma_u^+(v=0)$ and $X^2\Sigma_g^+(v=1)$ levels corresponding to the transition at 428 nm. The total probability of N_2 ionization is shown with a green dashed line. Laser parameters are the same as in Fig. 2.

Both 391 nm and 428 nm transitions share the same upper level $B^2\Sigma_u^+(v=0)$ but populations at lower levels are different. The $X^2\Sigma_g^+(v=0)$ level is populated abundantly by direct ionization, while the ionization probability at $X^2\Sigma_g^+(v=1)$ level is much smaller, see blue line in Fig. 2(a). Consequently, the threshold intensity for the 428 nm population inversion is smaller than that for the 391 nm one. In the intensity range of $(0.5-2.6)\times10^{14}$ W/cm^2, ionization injection into $X^2\Sigma_g^+(v=0)$ level dominates over the excitation probability, and thus emission only at 428 nm is allowed. For higher intensities, the ground level of N_2^+ ion is sufficiently depleted, thus opening the possibility for emission at 391 nm. At laser intensities above 4×10^{14} W/cm^2, the ionization depletion becomes severe around the maximum of the laser pulse, as shown by green dashed line in Fig. 4. In that case, ionization injection into $X^2\Sigma_g^+(v=0)$ level is very small during the remaining laser pulse, and populations at $A^2\Pi_u(v=2)$ and $B^2\Sigma_u^+(v=0)$ levels partially are repumped back to $X^2\Sigma_g^+(v=0)$ due to the near-resonance Rabi oscillation. This fact explains the decrease of 391 nm inversion at high intensities. The ionization depletion effect was not considered in Ref. [9], which explains their difference from our results.

Besides the 800 nm near-infrared laser experiments, the cavity-free N_2^+ lasing at 423 nm and 428 nm in air irradiated by a 400 nm ultraviolet intense laser pulse has been reported [30,31]. The

Optics EXPRESS

authors theoretically assumed a prompt ionization of N_2 into N_2^+ ground state at the peak of the laser pulse and ascribed the relevant population inversions to Rabi oscillation combined with a Raman-type transitions. The authors demonstrated this process by numerically solving TDSE for N_2^+ ion interacting with the second half of the laser pulse. In order to verify this interpretation, we performed simulations with the TDSE and DM models by accounting for the ionization and excitation processes and angle-averaging the populations at the end of the laser pulse. Figure 5(a) presents the intensity dependence of the population inversions for the laser wavelength λ=400 nm and pulse duration $\tau = 30\,T_{400}$. Both 428 nm (red) and 423 nm (green) transitions show an increase of inversion with the laser intensity for I>1.5 × 10^{14} W/cm^2. As expected, DM again underestimates the population inversions due to its instantaneous incoherent ionization injection. More simulations (not shown) confirm that the results are robust with respect to the laser pulse duration.

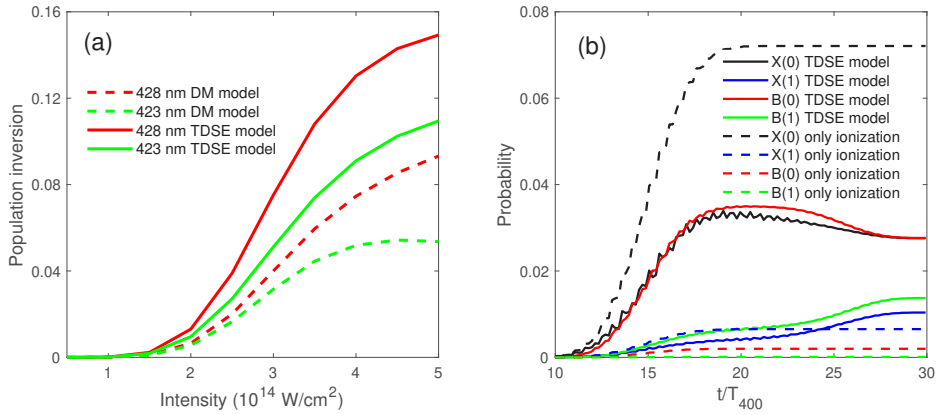

Fig. 5. (a). N_2^+ population inversion of the emissions at 428 nm [$B^2\Sigma_u^+(v=0) - X^2\Sigma_g^+(v=1)$, red] and 423 nm [$B^2\Sigma_u^+(v=1) - X^2\Sigma_g^+(v=2)$, green]. Solid and dashed lines represent TDSE and DM results, respectively. (b) N_2^+ time-dependent populations at the levels $X^2\Sigma_g^+$ ($v=0$ black, $v=1$ blue) and $B^2\Sigma_u^+$ ($v=0$ red, $v=1$ green) for the case of $\theta = 45°$. Solid lines show the TDSE results and the dashed show the case where only ionization is included. Laser parameters are: $\omega = 0.114$ a.u. ($\lambda = 400$ nm) and $\tau = 30\,T_{400}$ ($T_{400} = 55.13$ a.u.). The laser intensity in panel (b) is 2.0×10^{14} W/cm^2.

To better understand the reason of inversion, we trace in Fig. 5(b) the time dependence of the population at four levels for the case of molecular axis oriented at $\theta = 45°$ with respect to the laser polarization. The solid lines account for ionization and excitation of vibrational states, while the dashed lines account only for the ionization process. By comparing with black solid and dashed lines, it can be deduced that a large amount of population at $X^2\Sigma_g^+(v=0)$ produced through direct ionization is transferred to $B^2\Sigma_u^+(v=0,1)$ levels via the single photon transition. This single photon excitation combined with the instantaneous ionization injection gives rise to the 428 nm and 423 nm population inversions. Other excited levels, such as the $X^2\Sigma_g^+(v=1)$ participating Raman-type transition, make a small contribution in this case. Note that the state $A^2\Pi_u$ is hardly excited because of a large detuning.

4. Conclusion

We have studied the population at vibrational levels in N_2^+ under ionization and excitation with intense 800 nm and 400 nm laser pulses by using TDSE and DM models. The DM model underestimates the population probability due to the specific ionization condition corresponding

Optics EXPRESS

to mixed quantum states. This error can be corrected by an additional ionization condition (13) accounting for the off-diagonal component of the density matrix. Such an improved DM model could be used for fast and accurate calculations of population at excited states for various interaction conditions such as molecular rotational states.

Two particular laser wavelengths are considered. In the 400 nm case, the population inversion corresponding to 423 nm and 428 nm transitions is robust and appears at laser intensities above 1.5×10^{14} W/cm^2. The time-dependent population analysis provides an explanation of this effect as a single-photon near resonance transition between $X^2\Sigma_g^+$ and $B^2\Sigma_u^+$ states combined with the instantaneous ionization. In the 800 nm case, the population inversion corresponding to the 428 nm transition appears also at low intensities above 1.5×10^{14} W/cm^2. However, the population inversion corresponding to the 391 nm transition appears at higher intensities above 2.6×10^{14} W/cm^2 and it approaches a saturation above 4×10^{14} W/cm^2 because of a larger ionization Franck-Condon factor and the ionization depletion effect.

Funding. National Natural Science Foundation of China (12204308, 12034013, 11904232, 11925405, 91850203); Shanghai Municipal Education Commission (22ZR1444100); Innovation Program of Shanghai Municipal Education Commission (2017-01-07-00-07-E00007).

Acknowledgments. Authors are grateful to Maria Richter, Misha Ivanov, Hongbin Lei, and Jing Zhao for for the helpful and enlightening discussions.

Disclosures. The authors declare no conflicts of interest.

Data availability. Data underlying the results presented in this paper are not publicly available at this time but may be obtained from the authors upon reasonable request.

Supplemental document. See Supplement 1 for supporting content.

References

1. A. Dogariu, J. B. Michae, and M. O. Scully, "High-gain backward lasing in air," Science **331**(6016), 442–445 (2011).
2. J. Yao, B. Zeng, H. Xu, G. Li, W. Chu, J. Ni, H. Zhang, S. L. Chin, Y. Cheng, and Z. Xu, "High-brightness switchable multiwavelength remote laser in air," Phys. Rev. A **84**(5), 051802 (2011).
3. P. R. Hemmer, R. B. Miles, P. Polynkin, T. Siebert, A. V. Sokolov, P. Sprangle, and M. O. Scully, "Standoff spectroscopy via remote generation of a backward-propagating laser beam," Proc. Natl. Acad. Sci. U. S. A. **108**(8), 3130–3134 (2011).
4. J. Ni, W. Chu, H. Zhang, B. Zeng, J. Yao, L. Qiao, G. Li, C. Jing, H. Xie, H. Xu, Y. Cheng, and Z. Xu, "Impulsive rotational Raman scattering of N_2 by a remote "air laser" in femtosecond laser filament," Opt. Lett. **39**(8), 2250 (2014).
5. Z. Zhang, F. Zhang, B. Xu, H. Xie, B. Fu, X. Lu, N. Zhang, S. Yu, J. Yao, Y. Cheng, and Z. Xu, "High-sensitivity gas detection with air-lasing-assisted coherent Raman spectroscopy," Ultrafast Science **9**, 761458 (2022).
6. A. Laurain, M. Scheller, and P. Polynkin, "Low-threshold bidirectional air lasing," Phys. Rev. Lett. **113**(25), 253901 (2014).
7. S. Mitryukovskiy, Y. Liu, P. J. Ding, A. Houard, and A. Mysyrowicz, "Backward stimulated radiation from filaments in nitrogen gas and air pumped by circularly polarized 800 nm femtosecond laser pulses," Opt. Express **22**(11), 12750 (2014).
8. J. Yao, S. Jiang, W. Chu, B. Zeng, C. Wu, R. Lu, Z. Li, H. Xie, G. Li, C. Yu, Z. Wang, H. Jiang, Q. Gong, and Y. Cheng, "Population redistribution among multiple electronic states of molecular nitrogen ions in strong laser fields," Phys. Rev. Lett. **116**(14), 143007 (2016).
9. H. Xu, E. Lotstedt, A. Iwasaki, and K. Yamanouchi, "Sub-10-fs population inversion in N_2^+ in air lasing through multiple state coupling," Nat. Commun. **6**(1), 8347 (2015).
10. A. Azarm, P. Corkum, and P. Polynkin, "Optical gain in rotationally excited nitrogen molecular ions," Phys. Rev. A **96**(5), 051401 (2017).
11. Y. Liu, P. Ding, G. Lambert, A. Houard, V. Tikhonchuk, and A. Mysyrowicz, "Recollision-induced superradiance of ionized nitrogen molecules," Phys. Rev. Lett. **115**(13), 133203 (2015).
12. M. Richter, M. Lytova, F. Morales, S. Haessler, O. Smirnova, M. Spanner, and M. Ivanov, "Rotational quantum beat lasing without inversion," Optica **7**(6), 586 (2020).
13. H. Zhang, C. Jing, J. Yao, G. Li, B. Zeng, W. Chu, J. Ni, H. Xie, H. Xu, S. L. Chin, K. Yamanouchi, Y. Cheng, and Z. Xu, "Rotational coherence encoded in an "air-laser" spectrum of nitrogen molecular ions in an intense laser field," Phys. Rev. X **3**(4), 041009 (2013).
14. A. A. Svidzinsky, L. Yuan, and M. O. Scully, "Transient lasing without inversion," New J. Phys. **15**(5), 053044 (2013).

Optics EXPRESS

15. A. Mysyrowicz, R. Danylo, A. Houard, V. Tikhonchuk, X. Zhang, Z. Fan, Q. Liang, S. Zhuang, L. Yuan, and Y. Liu, "Lasing without population inversion in N_2^+," APL Photonics **4**(11), 110807 (2019).
16. J. Yao, L. Wang, J. Chen, Y. Wan, Z. Zhang, F. Zhang, L. Qiao, S. Yu, B. Fu, Z. Zhao, C. Wu, V. Yakovlev, L. Yuan, X. Chen, and Y. Cheng, "Photon retention in coherently excited nitrogen ions," Sci. Bulletin **66**(15), 1511–1517 (2021).
17. T. Ando, E. Lötstedt, A. Iwasaki, H. Li, Y. Fu, S. Wang, H. Xu, and K. Yamanouchi, "Rotational, vibrational, and electronic modulations in N_2^+ lasing at 391 nm: Evidence of coherent $B^2\Sigma_u^+$-$X^2\Sigma_g^+$-$A^2\Pi_u$ coupling," Phys. Rev. Lett. **123**(20), 203201 (2019).
18. H. Li, M. Hou, H. Zang, Y. Fu, E. Lötstedt, T. Ando, A. Iwasaki, K. Yamanouchi, and H. Xu, "Significant enhancement of N_2^+ lasing by polarization-modulated ultrashort laser pulse," Phys. Rev. Lett. **122**(1), 013202 (2019).
19. H. Li, E. Lötstedt, H. Li, Y. Zhou, N. Dong, L. Deng, P. Lu, T. Ando, A. Iwasaki, Y. Fu, S. Wang, J. Wu, K. Yamanouchi, and H. Xu, "Giant enhancement of air lasing by complete population inversion in N_2^+," Phys. Rev. Lett. **125**(5), 053201 (2020).
20. Q. Zhang, H. Xie, G. Li, X. Wang, H. Lei, J. Zhao, Z. Chen, J. Yao, Y. Cheng, and Z. Zhao, "Sub-cycle coherent control of ionic dynamics via transient ionization injection," Commun. Phys. **3**(1), 50 (2020).
21. V. Tikhonchuk, Y. Liu, R. Danylo, A. Houard, and A. Mysyrowicz, "Theory of femtosecond strong field ion excitation and subsequent lasing in N_2^+," New J. Phys. **23**(2), 023035 (2021).
22. V. Tikhonchuk, Y. Liu, R. Danylo, A. Houard, and A. Mysyrowicz, "Modeling of the processes of ionization and excitation of nitrogen molecules by short and intense laser pulses," Phys. Rev. A **104**(6), 063116 (2021).
23. S. R. Langhoff, C. W. Bauschlicher Jr., and H. Partridge, "Theoretical study of the N_2^+ Meinel system," J. Chem. Phys. **87**(8), 4716–4721 (1987).
24. S. R. Langhoff and C. W. Bauschlicher Jr., "Theoretical study of the first and second negative systems of N_2^+," J. Chem. Phys. **88**(1), 329–336 (1988).
25. J. Crank and P. Nicholson, "A practical method for numerical evaluation of solutions of partial differential equations of the heat-conduction type," Math. Proc. Cambridge Philos. Soc. **43**(1), 50–67 (1947).
26. X. M. Tong, Z. X. Zhao, and C. D. Lin, "Theory of molecular tunneling ionization," Phys. Rev. A **66**(3), 033402 (2002).
27. S.-F. Zhao, C. Jin, A.-T. Le, T. F. Jiang, and C. D. Lin, "Determination of structure parameters in strong-field tunneling ionization theory of molecules," Phys. Rev. A **81**(3), 033423 (2010).
28. R. Kosloff and H. Tal-Ezer, "A direct relaxation method for calculating eigenfunctions and eigenvalues of the Schrödinger equation on a grid," Chem. Phys. Lett. **127**(3), 223–230 (1986).
29. J. Chen, J. Yao, H. Zhang, Z. Liu, B. Xu, W. Chu, L. Qiao, Z. Wang, J. Fatome, O. Faucher, C. Wu, and Y. Cheng, "Electronic-coherence-mediated molecular nitrogen-ion lasing in a strong laser field," Phys. Rev. A **100**(3), 031402 (2019).
30. T. Wang, J. Daigle, J. Ju, S. Yuan, R. Li, and S. L. Chin, "Forward lasing action at multiple wavelengths seeded by white light from a femtosecond laser filament in air," Phys. Rev. A **88**(5), 053429 (2013).
31. S. Wang, E. Lotstedt, J. Cao, Y. Fu, H. Zang, H. Li, T. Ando, A. Iwasaki, K. Yamanouchi, and H. Xu, "Population inversion in N_2^+ by vibrationally mediated Rabi oscillation at 400 nm," Phys. Rev. A **104**(3), 032823 (2021).